Desalination and Water Treatment
www.deswater.com

doi: 10.5004/dwt.2017.20117

77 (2017) 1–18
May

Closed-circuit PRO series no. 6: advanced PRO membranes and technologies

Avi Efraty

Osmotech Ltd, P.O. Box 132, Har Adar 90836, Israel, Tel. +972-52-4765-687; Fax: +972-2-570-0262; email: efraty.adt@012.net.il

Received 18 October 2015; Accepted 1 February 2017

ABSTRACT

Recent advances in pressure-retarded osmosis (PRO) membranes are viewed and analyzed in the context of the closed-circuit PRO technology (CC-PRO) of near absolute energy conversion efficiency without need of an energy recovery device. The performance of an extended list of advanced PRO membranes in different salinity gradients is analyzed by means of their readily available permeability coefficient (A), actual/ideal forward osmosis flux ratio (β), and draw/permeation flow ratio (δ), and the results of this approach reveal consistent results with rigorous theoretical model calculations and experimental data. CC-PRO simulations on the basis of A, β, and δ illustrate the application this approach for the projection of flux, power density (PD), and net electric power density (NEPD) dependence on applied pressure for various advance PRO membranes with emphasis of their maximum PD and NEPD prospects and the distinction between these terms. NEPD takes into account the power demand of the auxiliary pumps in the PRO system and, therefore, represents the actual power availability of such systems. Experimental PD results derived from small lab-bench systems are shown to be consistent with the A–β CC-PRO simulated projections of high flow ratio ($\delta > 40$), which correlate to maximum PD of negative NEPD and, therefore, inappropriate for an effective PRO operation. The relationship of PD and NEPD is exemplified for the seawater brine and river water like salinity gradient system using an effective PRO membrane with $\beta = 0.447$ and the simulated CC-PRO results revealed maximum PD of 21.8 W/m^2 at 23 bar and $\delta = 40$ under which conditions NEPD is (–)31.8 W/m^2; whereas maximum NEPD of 10.0 W/m^2 is attainable at 26 bar and $\delta = 3$. Apart from the application of the simple A–β method for power projections of advanced thin film composites PRO membranes, this study also appraises the PRO technology as a standalone or in hybrid forms for practical applications in different salinity gradients.

Keywords: PRO; Closed-circuit PRO; Power density; Net electric power density; Actual/ideal FO flux ratio (β); Draw/permeation flow ratio (δ) of PRO membranes

1. Introduction

Global climate changes inflicted by adverse green-house effects due to power generation from combustible fossil fuels, also cause depletion/deterioration of existing groundwater and surface water sources in various part of the world resulted. The aforementioned, viewed in the context of the rapidly expanding global population, suggest urgent needs for the development of new large-scale clean power generation technologies and modern low-energy techniques for freshwater production. Energy and freshwater aspects are interrelated issues, since enhancement of the global green-house effect also contributes to increased arid zones in various regions on earth of declined freshwater availability with needs to desalinate seawater by energy-rich processes in order to meet demand of growing populations. Today, estimated 92% of the global electric power demand is generated from combustible fuels; 5.2% originates from nuclear reactors; 2.3% from hydroelectric power stations, and only 0.5% from wind/solar/geothermal natural clean energy sources. Nuclear power generation has declined over the past decades due to several disastrous events; hydroelectric power generation is confined by the availability of suitable rivers' sites; harvesting of wind power economically is conditioned by availability of wind regimes of sufficient wind velocity and frequency; harvesting of solar power with solar panels provides low power output only during day time and requires large surface area; and geothermal power generation proceeds with low efficiency only in isolated locations. Unless controlled, the progression of the green-house effect will

ultimately lead to the devastation of the human civilization, and this course of events could be stopped only if a major fraction of the present global power production will shift from combustible fossil fuels to non-combustible clean energy sources, a process which has already began but needs to be accelerated in order to become effective.

Since the inception of reverse osmosis (RO) applications for desalination some 60 years ago [1], membrane-based technologies have became widespread worldwide for large-scale water treatment and/or for low-energy freshwater production from seawater [2]. By analogy with RO, the opposite membrane-based spontaneous process of forward osmosis (FO) in the form of pressure-retarded osmosis (PRO) could provide a plausible route to large-scale clean energy generation from salinity gradients of natural occurrence (e.g., sea–river water like) or man-made (e.g., seawater brine and treated domestic effluents [TDE]). Since first reported by Loeb in 1975 [2–5], the development of the membrane-based PRO approach to clean power generation has gained an enormous momentum during the past decade evident by the increased number of general studies and review articles [2,6–18], which cover all major aspects in the developments of advanced FO and PRO membranes, including the understanding of their behaviors and ultimate prospective applications. Compared with RO, FO and PRO processes proceed with much greater complexity due to detrimental effects on flux, and the development of such processes requires fabrication of new effective membranes of low detrimental effects and the evaluation of their properties by experimental techniques as well as by rigorous theoretical models studies. The accumulation of experimental and theoretical knowledge on FO and PRO membranes enabled to identify the origin and magnitude of the principal detrimental effects and suggested the ways and means to create better membranes of higher power output. Reports of newly prepared PRO membranes normally consist of detailed fabrication procedures; determination of their permeability coefficients (A, LMH/bar), salt diffusion coefficients (B, LMH), and structural parameters (S, μm); rigorous theoretical model projections of flux and power density (PD) as function of hydraulic pressure difference (Δp) referred hereinafter as applied pressure (AP); and the experimental validation procedures of theoretical flux and PD projections by means of lab-bench systems. Rigorous theoretical model calculations of different PRO membranes are not necessarily identical, although similar and based on the same A, B, and S parameters with adjustments intended to create a better agreement with experimental results, which in most instances are not provided duplicates. Most obviously, the fabrication and characterization of new PRO membranes is an extensive interdisciplinary task of considerable complexity covering synthetic, chemical, physical, structural, and theoretical aspects of material science related to the properties of semi-permeable surfaces and their support layers.

Effective PRO hydroelectric power generation depends on the characteristics of membranes, module performance, and technology selection. The present study focuses on the newly conceived closed-circuit PRO (CC-PRO) technology [19] of near absolute energy conversion efficiency without need for an energy recovery device (ERD) and its prospective applications in different salinity gradients [20–24] according to theoretical model simulations on the basis of the permeability coefficient (A) of membranes and their actual/ideal flux ratio (β) under FO conditions as well as by accounting for the "draw"/permeation flow ratio (δ), which determines the stationary-state conditions inside of PRO modules.

2. Conventional and closed-circuit PRO (CC-PRO)

In contrast to Loeb's conventional PRO apparatus of the schematic design in Fig. 1 with an ERD in its center, the new CC-PRO technology [19] proceeds by means of pressurized "draw" solution (henceforth – HSF, high salinity feed) supplied in closed circuit at module inlet, under the intrinsically created osmotic pressure of choice as an AP, through the alternately engaged side conduits (SC) in an apparatus according the schematic design displayed in Fig. 2. The engaged SC releases HSF and accepts the high salinity diluted feed (henceforth – HSDF) simultaneously, and near the end of the HSF release the engaged SC is replaced by the alternating SC, which is fully charged with HSF and compressed. After disengagement, the SC is decompressed; HSDF replaced by HSF at near atmospheric pressure, and then the fully charged SC is sealed, pressurized by connecting to the closed circuit at one end, and left on stand-by for the next engagement. The decompression/compression steps of the SC during recharge take place hydrostatically with negligible energy requirements, and therefore, the entire CC process proceeds with near absolute energy conversion efficiency without need for ERD. The various design and performance aspects of the CC-PRO technology have already been discussed at length elsewhere [20–24], and emphasis hereafter shall relate to specific issues. The intrinsic volume of the closed circuit in CC-PRO is fixed, and this implies that the only outlet for the permeation flow (Q_p) is through the turbine-generator (T-G), as well as that the HSF flow rate at module inlet (Q_i) is controlled by the circulation pump (CP). The stationary-state conditions created

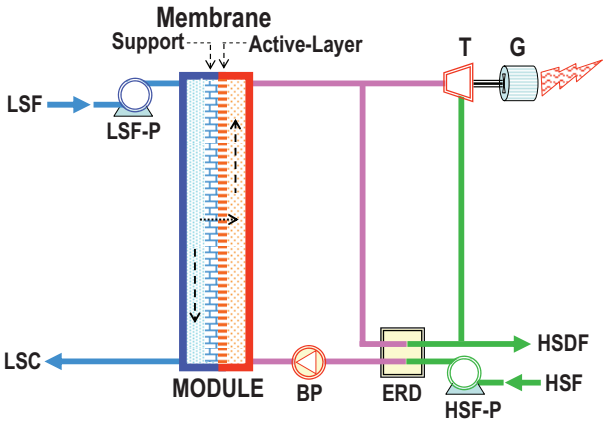

Fig. 1. Schematic design of a single module conventional PRO apparatus and its essential components.
Note: LSP – low salinity feed ("feed" solution); LSC – low salinity concentrate (concentrated "feed" effluent); HSF – high salinity feed ("draw" solution); HSDF – high salinity diluted feed (diluted "draw" solution); T – turbine; G – generator; HSF-P – high salinity feed pump; LSF-P – low salinity feed pump; BP – booster pump; and ERD – energy recovery device.

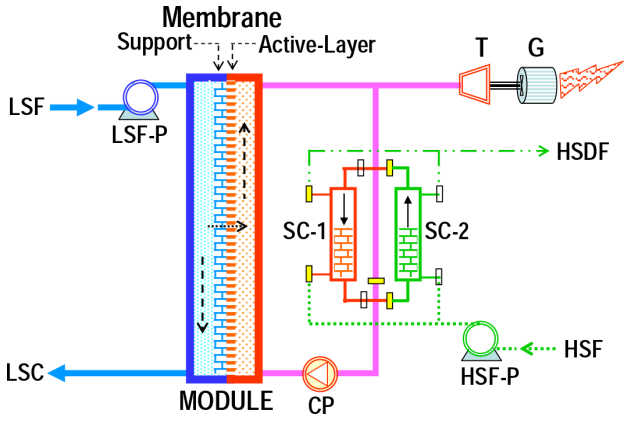

Fig. 2. Schematic design of a single module CC-PRO apparatus and its essential components.
Note: LSP – low salinity feed ("feed" solution); LSC – low salinity concentrate (concentrated "feed" effluent); HSF – high salinity feed ("draw" solution); HSDF – high salinity diluted feed (diluted "draw" solution); T – turbine; G – generator; HSF-P – high salinity feed pump; LSF-P – low salinity feed pump; CP – circulation pump; and SC – side conduit.

inside the module under CC-PRO are determined by the HSF/permeation flow ratio (δ) expressed by Eq. (1) with average flux expressed by Eq. (2) and average power density (PD_{av}) by Eq. (3); where p_{ap} stands for AP, $\Delta\pi_{av}$ for the average osmotic pressure difference along the module (inlet to outlet average), and β for the actual (J_{ac})/ideal (J_{id}) water flux ratio expressed by Eq. (4) for defined membrane and salinity gradient. Since Q_i is the controlled flow rate of CP and the osmotic pressure gradient along the module and its average ($\Delta\pi_{av}$) can be determined from the flow ratio (δ) and HSF concentration of known constituents, this implies that J_{av} and PD_{av} curves as function of p_{ap} can be derived by the knowledge of A, β, δ, and the concentrations of the HSF and LSF solutions, and this approach in the context of CC-PRO theoretical model simulations has already been cited elsewhere [20–24].

$$\delta = Q_i / Q_p \tag{1}$$

$$J_{av} = \beta \times A \times \left(\Delta\pi_{av} - p_{ap}\right) \tag{2}$$

$$PD_{av} = \left(1/36\right) \times J_{av} \times p_{ap} = \left(1/36\right) \times \beta \times A \times \left(\Delta\pi_{av} - p_{ap}\right) \times p_{ap} \tag{3}$$

$$\beta = J_{ac} / J_{id} \tag{4}$$

Conventional PRO (Fig. 1) differs from CC-PRO (Fig. 2) by the presence of ERD instead of SC. The SCs in CC-PRO are enlarged diameter conduit sections of the closed circuit, and the flow inside the closed circuit is driven by CP, which also compensates for the flow-induced pressure losses along the module, which are normally relatively small. In case of conventional PRO (Fig. 1), the BP compensates for the flow-induced pressure losses along the module as well as for the pressure losses encountered in the pressure exchanger (ERD) with the latter being considerably higher. In contrast to the near absolute energy conversion efficiency of CC-PRO due to negligible compression/decompression energy losses, the energy conversion efficiency in conventional PRO depends on the efficiency of the integrated ERD in the system, and such information was not disclosed in the reported performance of the demonstration units with PX-ERD in Norway [25–27] and/or Japan [28–30], although such information was most obviously available. Advanced ERD means (e.g., pressure exchanger (PX) and dual work exchanger energy recovery (DWEER)) are extensively used in large modern SWRO desalination plants in order to improve their energy efficiency by energy recovery from the disposed pressurized brine. In the SWRO Palmachim mega-plant in Israel, which is equipped with an advanced ERD-PX hybrid ERD system, the energy conversion efficiency was reported [31] to be "just over 76% at the best efficiency point" and less below the referred point, and similar estimates were shown [32] to be true by analyzed data of several other large plants. If energy conversion efficiency of 76% or less is typical of SWRO desalination plants with advanced ERD means where brine flow is about half that of the feed, the application of such means in the context of conventional PRO should lead to even greater energy losses since recovery is required from the entire HSF flow, not half as in case of SWRO. The aforementioned implies that CC-PRO, which saves the need for expensive ERD means, should allow a greater power output of 25%–40% compared with conventional PRO. The combination of lower installation costs and greater power output should make CC-PRO the method of choice for all future PRO applications.

3. Performance evaluation of PRO membranes

The permeability (A) and salt diffusion (B) coefficients are the footprints of semi-permeable membranes and yield satisfactory RO projections when apply in the context of the theoretical RO equations [33]. In contrast to RO, PRO is by far a more complex process influenced by external concentration polarization (ECP) on both sides of the semi-permeable membrane, internal concentration polarization (ICP) due to the membrane's support, and the structural features of the membrane manifested by the S parameter and expressed by Eq. (5), where t_s stands for support thickness, τ for support tortuousness and ε for support porosity. The S parameter expresses the distance that a solute particle needs to pass from the active layer to the bulk of the feed solution. Theoretical performance simulation of PRO membranes assumes models that take into account the A, B, and S parameters; water flux as function of Δπ – Δp (osmotic less hydraulic pressure differences across the membrane); reverse solute flux as function of the salinity gradient across the membrane; and adjustments to allow good agreement with experimental results. Rigorous theoretical model simulations need to be validated by trustworthy experimental results. PRO experimental results are normally expressed in the forms of flux and PD projections as function of AP, wherefrom maximum PD at a defined AP is clearly distinguished per given membrane and salinity gradient. The ratio of water flux (J_w) to solute flux (J_s), also known as water/salt flux selectivity, in PRO is expressed by Eq. (6) [17], where k stands for the van't Hoff constant, R for the ideal gas constant, and T for the absolute temperature.

According to Eq. (6), the water/salt selectivity is independent of the structural parameter of the membrane and the concentration of the HSF "draw" solution, with greater water flux and PD expected by increased *A*, decreased *B*, and a "draw" solution of a higher osmotic pressure.

$$S = t_s \times \tau/\varepsilon \tag{5}$$

$$J_w/J_s = \left(A/B\right) \times k \times R \times T \tag{6}$$

PRO experiments are commonly carried out by small lab-bench systems operated under high "draw"/permeation flow ratio (δ > 35) conditions with recycled HSF ("draw") and LSF ("feed") solutions, and this implies a progressive change in the concentrations of both HSF and LSF at module inlet during experimental trials. Moreover, most of the reported PRO flux and PD experimental results are provided without duplicates to show data reproducibility and, therefore, should be viewed with caution. Many reported experimental results are limited to the low-range AP, well below the AP of peak power, in which cases the validation of peak power from rigorous theoretical model calculations is not possible. Since most PRO experiments are carried out under high flow ratio (δ) of maximum power availability due to small module inlet→outlet gradients as well as under changing stationary-state conditions inside the module due to HSF and LSF recycling; therefore, experiment results under such conditions do not provide typical information of a common single-pass PRO process, which normally takes place under a much lower flow ratio (δ) with 30%–50% permeates in HSDF, a parameter solely defined by δ. Experimental data at high δ (>35) pertain to HSDF with less than 2.5% permeates with maximum PD projections being significantly higher compared those under common single-pass processes with 30%–50% permeates in HSDF of much lower δ (3→1). The development and performance characterization of FO and PRO membranes have received considerable attention in recent years and are summarized in several noteworthy general studies and review articles [2,7–16] wherein the various aspects mentioned hereinabove are covered rather comprehensibly. Although based on solid theoretical grounds and experimental principles, the existing performance evaluation techniques of PRO membranes are complex, time consuming, expensive, and do not necessarily provide practical PRO performance information, and for these reasons the need for simple reliable evaluation techniques of newly fabricated PRO membranes is imminent, and one such technique is discussed hereinafter.

Since FO and PRO are analogous processes, it was assumed as first approximation that both are controlled by same detrimental effects, or in simple terms, that the same membrane actual/ideal flux ratio (β) in FO also applies for flux and PD projections under PRO conditions. Model uniformity of FO and PRO is implied by the fact that FO and PRO flux at zero AP are identical terms and manifest the highest possible water flux and solute flux in the opposite directions at module, and in case of PRO, such flux is expected to decline as linear function of AP as implied by the general flux expression $J_w = A \times (\Delta\pi - p_{ap})$, where Δπ is a linear function of the solute concentrations according to the van't Hoff equation. The aforementioned assume that the actual/ideal flux ratio (β) at module inlet is maintained during the PRO progression even when AP is raised as long as the concentrations of HSF "draw" and LSF "feed" solutions at module inlet remain unchanged, since the intrinsic footprints of the membrane (*A* and *B* coefficients and the *S* parameter) remain unchanged.

The actual/ideal flux ratio (β) in FO per given membrane and salinity gradient is readily determined according to Eq. (4) from the measured FO flux (J_{ac}) with ideal flux (J_{id}) calculated according to Eq. (2) for p_{ap} = 0, β = 1.0, and the osmotic pressure gradient at module inlet ($\Delta\pi_i$) derived from the HSF and LSF concentrations by the van't Hoff equation. Incidentally, the knowledge of *A*, β, $\Delta\pi_i$, and the permeation flow (Q_p, L/h) also allow to determine the membrane effective surface (MES, m²) by means of Eq. (7); where Q_p is expressed by Eq. (8) and determined by flow meters or by LSF inlet–outlet weight difference.

$$\text{MES} = Q_p/(\beta \times A \times \Delta\pi_{\text{ideal}}) \tag{7}$$

$$Q_p = Q_{\text{HSDF}} - Q_{\text{HSF}} \tag{8}$$

The validity of the *A*–β method for the fast performance evaluation of PRO membranes was studied by the generations of flux and PD projection curves on the basis of reported experimental flux information for the advanced PRO thin film composites (TFC) membranes MP#1 by Yip et al. [34]; Hydration Innovation Technology (HIT)-TFC by Straub et al. [35]; PA-PES by Chou et al. [36]; PES-*A* and PES-*B* by Zhang and Chung [37]; TFC-PES by Wan and Chung [38], and TNC-1, TNC-2 and TNC-3 by Song et al. [39] for which rigorous theoretical model projections were also available. The summary of results is furnished in Table 1 and provides a comprehensive comparison between the maximum PD projections and their peak power pressures for the cited PRO membranes in different NaCl salinity gradients derived by rigorous theoretical model calculations (henceforth "rigorous" method) on the basis of *A*, *B* and *S* as well as by the *A*–β method on the basis of *A* and the readily available FO actual/ideal flux ratio (β). Comparison between maximum PD projections of the cited PRO membranes (Table 1) in defined salinity gradients by the rigorous and the *A*–β methods are displayed in Fig. 3, and a similar comparison of peak power pressures is displayed in Fig. 4. Maximum PD projections by the rigorous and *A*–β methods as function of β (Fig. 5(a)); AP at maximum PD (Fig. 5(b)); salinity gradient (Fig. 5(c)); permeability coefficient (Fig. 5(d)); salt diffusion coefficient (Fig. 5(e)); and structural parameter (Fig. 5(f)) reveal near equivalent or similar data points, implying that the actual/ideal flux ratio term (β) manifests the combined detrimental effects as derived by rigorous model calculations on the basis of the *A* and *B* coefficients and the *S* parameter. The dependence of β on feed salinity for membranes of the same *A*, *B* and *S* parameters is displayed in Fig. 6 as function of molar (a) and percentage concentrations (b).

The data points in Table 1, Figs. 3, 4, and 5(a)–(f) of maximum PD and peak power pressure were generated by the rigorous and *A*–β methods independently using basic membranes' information such as RO coefficients (*A* and *B*), structural parameter (*S*) and the FO actual/ideal flux ratio (β) in

Table 1
Maximum PD and applied pressure at peak power projections for various advanced PRO TFC membranes derived by the *A*–β method and by theory rigorous model calculations on the basis of *A*, *B*, and *S*

PRO membrane		Membranes parameters			Gradient system		Theory maximum power projections			*A*–β method maximum power projections			
Name	Type	*A*, LMH/bar	*B*, LMH	*S*, μm	HSF-draw, M NaCl	LSF-feed, M NaCl	W/m²	bar	REF	β	W/m²	bar	REF
MP#1	FS	5.81	0.88	349	0.55	0.001	10.0	12.5	34	0.374	10.0	13.0	21,22
HTI-TFC	FS	2.49	0.39	564	0.60	0.000	6.9	14.0	35	0.570	7.8	14.0	23,24
HTI-TFC	FS	2.49	0.39	564	1.00	0.000	15.0	25.0	35	0.341	14.4	24.0	23,24
HTI-TFC	FS	2.49	0.39	564	2.00	0.000	41.0	57.0	35	0.191	40.9	56.0	23,24
HTI-TFC	FS	2.49	0.39	564	3.00	0.000	74.0	91.0	35	0.123	76.0	94.0	23,24
PA-PES	HF	3.32	0.14	460	0.50	0.010	9.0	14.0	36	0.519	6.3	11.0	21
PA-PES	HF	3.32	0.14	460	0.75	0.010	18.0	23.0	36	0.413	11.0	17.0	21
PA-PES	HF	3.32	0.14	460	1.00	0.010	28.0	31.0	36	0.335	17.0	23.0	21
PES-*B*	HF	3.30	0.31	450	1.00	0.000	28.0	28.0	37	0.447	23.0	24.0	21
PES-*A*	HF	4.00	1.16	450	1.00	0.000	24.0	24.0	37	0.358	22.0	23.0	21
TFC-PES	HF	3.50	0.28	455	0.81	0.000	22.4	22.0	38	0.379	18.8	20.0	PS
TFC-PES	HF	3.50	0.28	455	0.81	0.011	17.0	23.0	38	0.525	12.9	19.0	PS
TNC-1	HF	1.23	0.28	149	1.06	0.009	13.1	24	39	0.591	13.5	26	PS
TNC-2	HF	3.82	1.19	135	1.06	0.009	21.3	22.8	39	0.363	25.8	26	PS
TNC-3	HF	5.31	3.86	140	1.06	0.009	20.2	20.4	39	0.272	26.9	26	PS
TNC-1	HF	1.23	0.28	149	1.06	0.080	10.2	24	39	0.489	9.6	24	PS
TNC-2	HF	3.82	1.19	135	1.06	0.080	15.2	22.8	39	0.260	15.8	24	PS
TNC-3	HF	5.31	3.86	140	1.06	0.080	14.4	20.4	39	0.190	16.02	24	PS

Note: FS – flat sheet; HF – hollow fiber; NA – not available; and PS – present study.

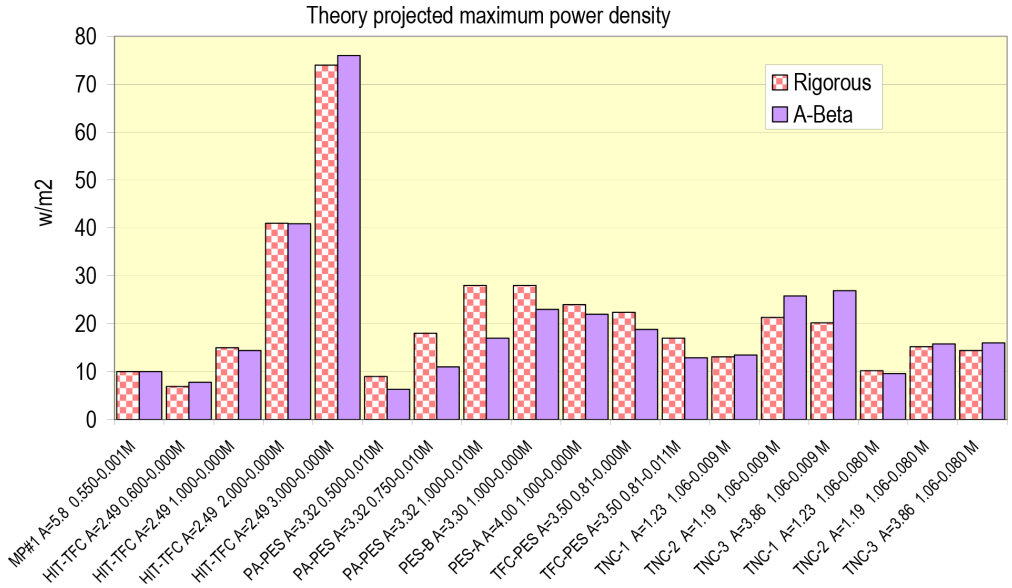

Fig. 3. Comparison between maximum PD projections for advanced PRO TFC membranes in defined salinity gradients derived by rigorous theoretical model calculation on the basis of *A*, *B* and *S*, and by the *A*–β method on the basis of *A* and the readily available FO actual/ideal flux ratio (β).

the latter case. Both procedures provide the means to generate complete flux and PD curves as function of AP and such comparative information is displayed in Fig. 7 for the MP#1 membrane in the 0.55–0.001 M NaCl salinity gradient with a continuous *A*–β curve [22] at high flow ratio (δ > 40) together with data points along said curve by the rigorous method according to the report by Yip et al. [34]. The high consistency between the *A*–β and rigorous projections displayed in

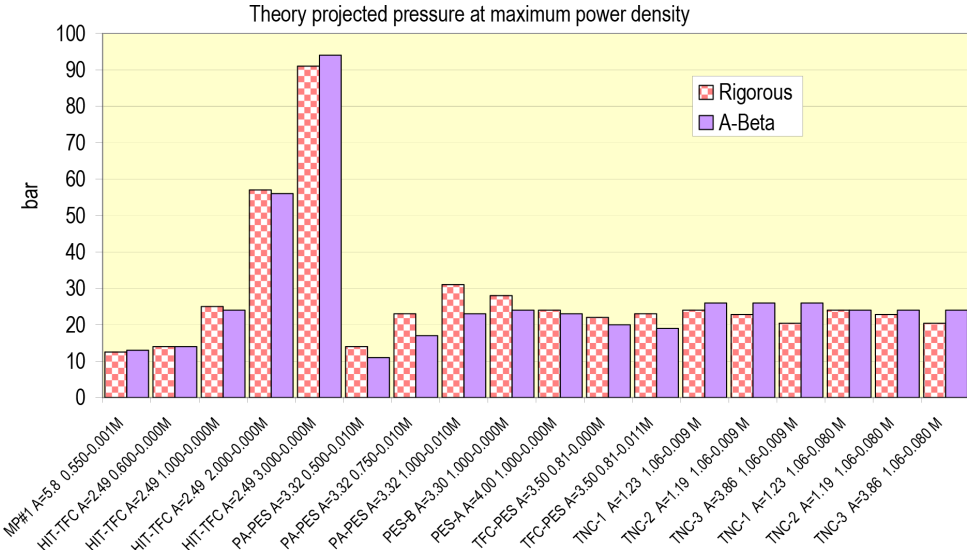

Fig. 4. Comparison between peak pressure of maximum power projections for advanced PRO TFC membranes in defined salinity gradients derived by rigorous theoretical model calculation on the basis of *A*, *B* and *S*, and by the β-*A* method on the basis of *A* and the readily available FO actual/ideal flux ratio (β).

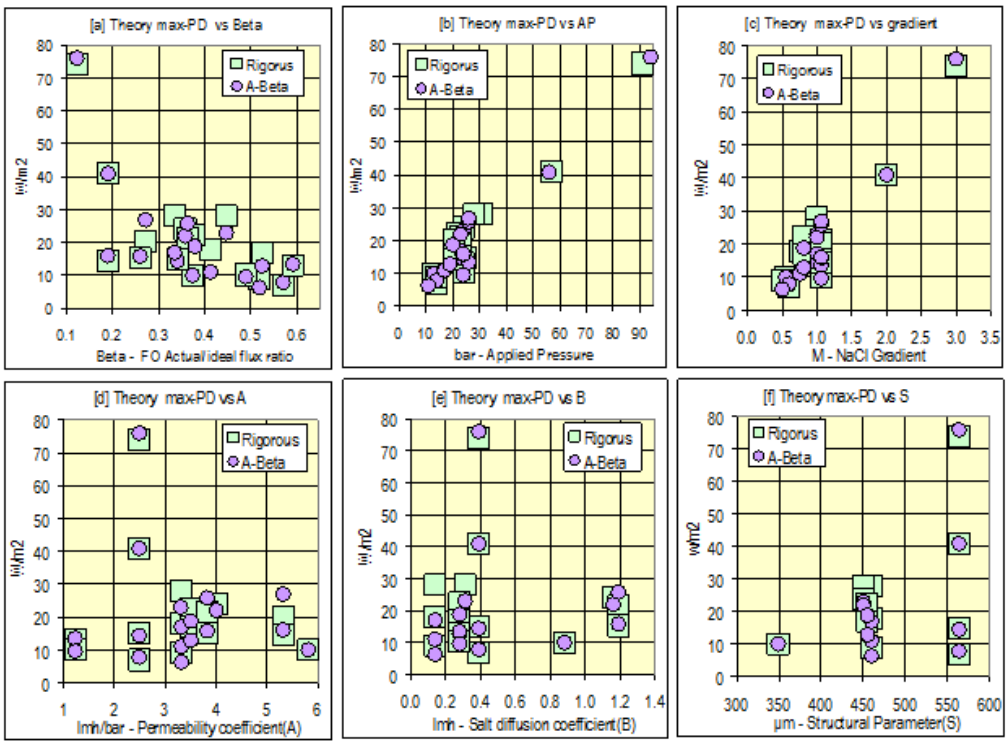

Fig. 5. Maximum PD projections for advanced PRO TFC membranes by the *A*–β and rigorous methods as function of β (a); applied pressure at maximum PD (b); salinity gradient (c); permeability coefficient (d); salt diffusion coefficient (e); and structural parameter (f) according to the data in Table 1.

Fig. 7 implies similar results by both approaches. A maximum PD curve projection by the *A*–β method, such as in Fig. 7, is based solely on the knowledge of the permeability coefficient (*A*), the actual/ideal FO flux ratio (β), and the salinity gradient at module inlet. In case of PD projections in general, the change in salinity between module inlet and outlet concentrations is defined by the HSF ("draw") concentration and δ, with increased δ manifesting a decreased salinity difference along the module concomitant with declined percentage of permeate in the HSDF (diluted "draw") effluent. Since the

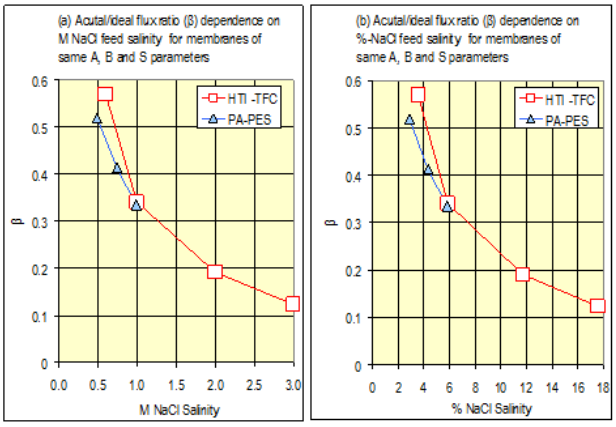

Fig. 6. Actual/ideal flux ratio (β) dependence on feed salinity gradient express in M NaCl (a) and % NaCl (b) for advanced PRO TFC membranes of the same *A*, *B*, and *S* parameters according to the data in Table 1.

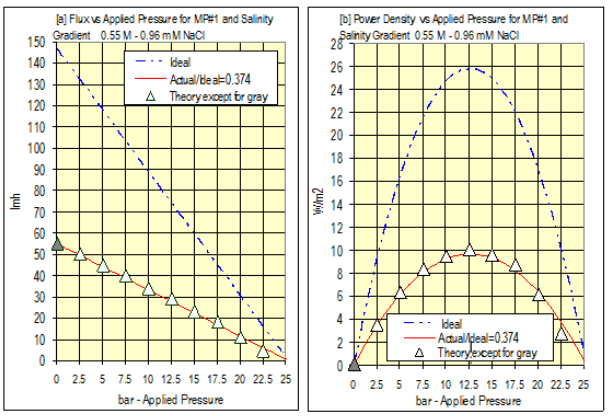

Fig. 7. Maximum PRO flux (a) and PD (b) projection curves for MP#1 in 0.550–0.001 M NaCl by the *A*–β (0.374) method at δ = 40 compared with the results of rigorous model calculation [34].

basic membranes' footprints (*A*, *B* and *S*) are not expected to change during a PRO process and the flux decline as function of increased AP is linear according to Eq. (2), as exemplified in Fig. 7(a) for the MP#1 membrane, this also implies an unchanged β during the PRO progression of declined salinity and flux along the module. In simple terms, the same β should apply to actual flux projection curves irrespective of δ and, thereby, allow PD projections in general and not only under stationary-state conditions of maximum PD as expected at high δ flow ratio. In this context, it should be pointed out that currently available experimental PD data are derived from flux measurements in small lab-bench systems under high flow ratio conditions and express maximum PD, which is unattainable under ordinary PRO operational conditions of much lower flow ratio. In light of the aforementioned, the *A*–β method provides a simple tool to generate flux and PD projections of general application for PRO membranes per each desired operational flow ratio (δ) and, thereby, circumvent the needs to determine structural parameters of membranes and engage in complex theoretical model calculation, which take into account issues such as the dilutive and concentrative ECP effects, dilutive and concentrative ICP effects associated with the porous support, reverse salt diffusion effects, and structural impact of membranes on the water flux and reverse salt diffusion processes. Since *A*, β, δ, and the salinity gradient at module inlet are basic parameters available right from start, therefore, their applications in the context of the *A*–β method greatly facilitate the performance evaluation of newly fabricated PRO membranes as first scan before committing to further investigations.

While the data in Fig. 7 for MP#1 pertain to the *A*–β and rigorous model calculation methods, noteworthy in particular are the β-projection curves vs. experimental results displayed in Figs. 8–14 for various PRO membranes in different salinity gradients. The most extensive reported study in this area by Straub et al. [35] pertains to experimental PD results for the HTI-TFC membrane in relationship to the β projections at δ = 40 displayed in Figs. 8(a)–(d) for the salinity gradients 0.6 (a); 1.0 (b); 2.0 (c); and 3.0 (d) M NaCl. Similar PD β curves in relationship to experimental results are provided in Figs. 9(a)–(c) for PA-PES by Chou et al. [36] in the 0.500–0.010 (a), 0.750–0.010 (b), and 1.000–0.010 (c) M NaCl salinity gradients; in Fig. 10(a)–(b) for PES-*A* (a) and RES-*B* (b) by Zhang and Chung [37] in the 1.000–0.000 M NaCl salinity gradient; in Figs. 11(a) and (b) for TFC-PES by Wan and Chung [38] in the 0.810–0.000 (a) and 0.810–0.011 (b) M NaCl salinity gradients; in Figs. 12(a) and (b) for TNC-1 by Song et al. [39] in the 1.060–0.009 (a) and 1.060–0.080 (b) M NaCl salinity gradients; in Figs. 13(a) and (b) for TNC-2 by Song et al. [39] in the 1.060–0.009 (a) and 1.060–0.080 (b) M NaCl salinity gradients; and in Figs. 14(a) and (b) for TNC-3 by Song et al. [39] in the 1.060–0.009 (a) and 1.060–0.080 (b) M NaCl salinity gradients. The good agreement between the PD β projections at high flow ratio (δ = 40) and experimental results derived from small lab-bench systems is self-evident from the data displayed in Fig. 8 for HTI-TFC; Fig. 9 for PA-PES; Fig. 10 for PES-*A* and PES-*B*; and Fig. 12 for TNC-1. The experimental PD results for TFC-PES in Figs. 11(a) and (b) show good agreement with β projections, except at peak power where the experimental results are somewhat higher (~5% (a) and ~14% (b) W/m^2). However, it should be noted in the case of Figs. 11(a) and (b) that the peak experimental data points rise above the expected shallow region of maximum, and in the absence of duplicates, it would appear difficult to assess the origin of the cited differences. In reference to the TNC-1 (Figs. 12(a) and (b)), TNC-2 (Figs. 13(a) and (b)), and TNC-3 (Figs. 14(a) and (b)) membranes, it should be noted that the rigorous model theoretical PD curves reported by Song et al. [39] are consisted with the β projections in the cited figures and that the discrepancy with experimental results for TNC-2 (Figs. 13(a) and (b)) and TNC-3 (Figs. 14(a) and (b)) originates from the procedure of preparation of said membranes. The TNC-1, TNC-2, and TNC-3 membranes constitute a unique class made of a thin-film nano-fiber composite with support structural properties of low tortuousness and high porosity that were modified by exposure to NaClO concentrations of 200 ppm (2 min), 1,000 ppm (1 h), and 2,000 ppm (2 h), respectively. The sharp decrease in experimental PD compared with the rigorous and β projections with increased exposure to NaClO most probably implies pressure-induced fundamental changes in the basic properties of the membranes, and from the reported data [40], it is not entirely clear whether such changes are reversible or not.

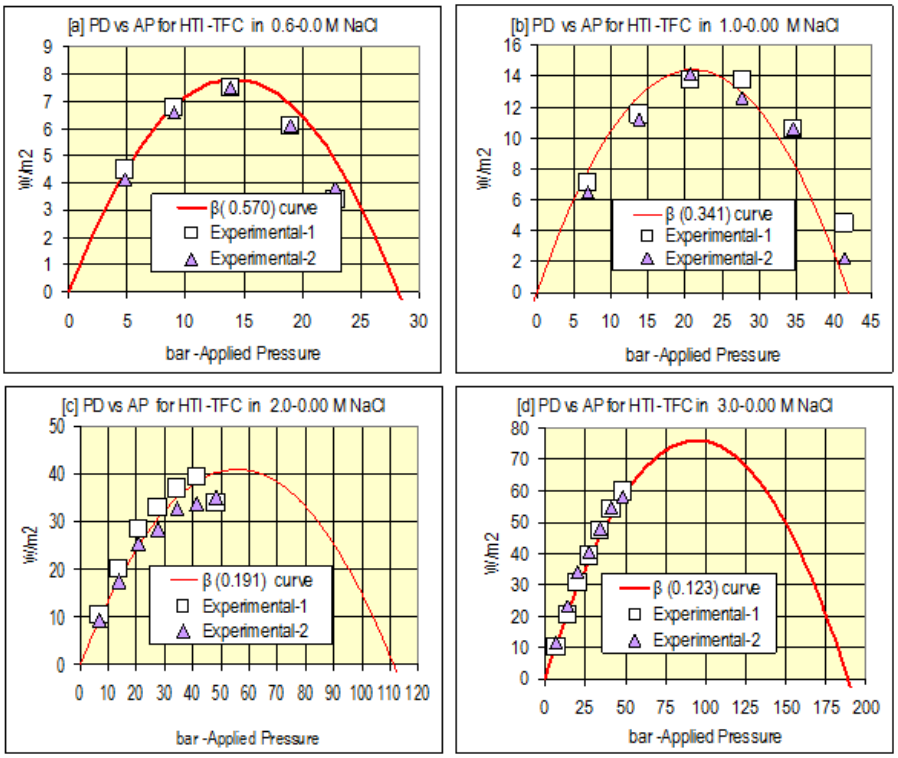

Fig. 8. Maximum PD projections for HTI-TFC at δ > 40 in the 0.6 (a); 1.0 (b); 2.0 (c); and 3.0 (d) M NaCl salinity gradients compared with reported [35] experimental results in duplicates.

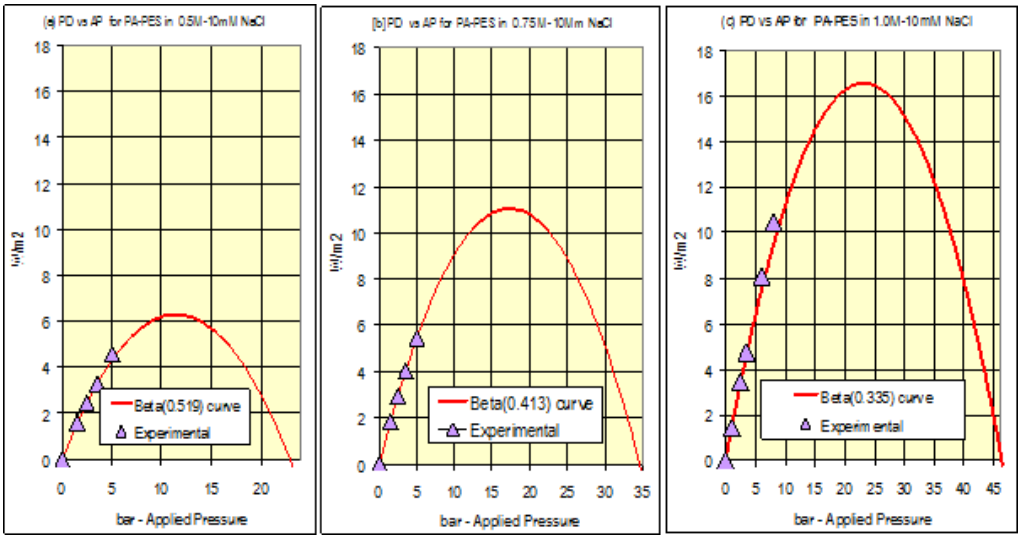

Fig. 9. Maximum PD β projections for PA-PES at δ > 40 in the 0.500–0.010 (a); 0.075–0.010 (b); and 1.000–0.010 (c) M NaCl salinity gradients compared with reported [36] experimental results.

Three noteworthy comments are warranted concerning the power projections considered hereinabove in reference to experimental data: first, power projection of peak power requires experimental validation in the peak power region, and such data are not always available. Second, experimental data from lab-bench set-up system are commonly generated under high flow ratio (δ), using recycled HSF ("draw") and LSF ("feed") solutions and, therefore, with continuously changing stationary-state conditions inside the PRO module. Third, experimental data generated at high flow ratio (δ) pertain to conditions of maximum PD of limited net electric power density (NEPD) availability in light of the high power demand of the auxiliary pumps in the PRO system. Accordingly, maximum PD projections and experimental

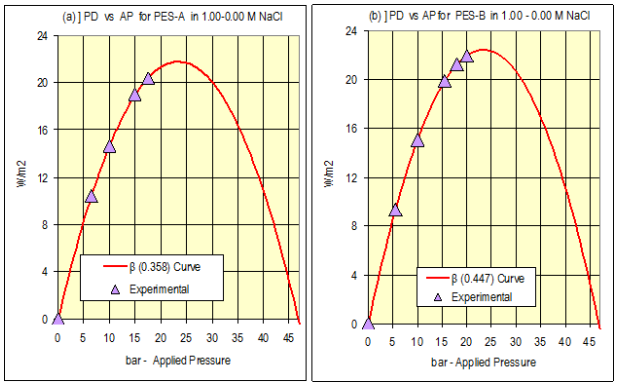

Fig. 10. Maximum PD β projections for PES-*A* (a) and PES-*B* (b) at δ > 40 in 1.000–0.000 M NaCl compared with reported [37] experimental results.

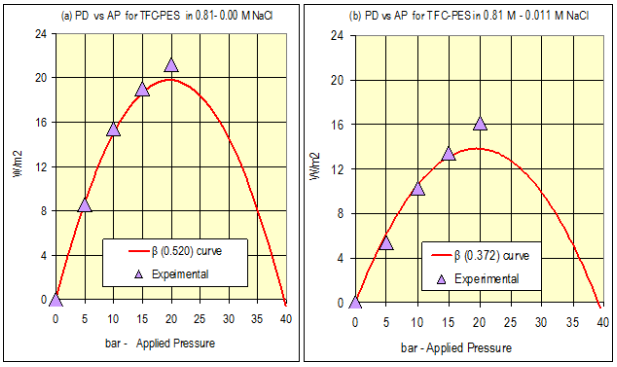

Fig. 11. Maximum PD β projections for TFC-PES at δ > 40 in 0.810–0.000 (a) and 0.81–0.011 (b) M NaCl compared with reported [38] experimental results.

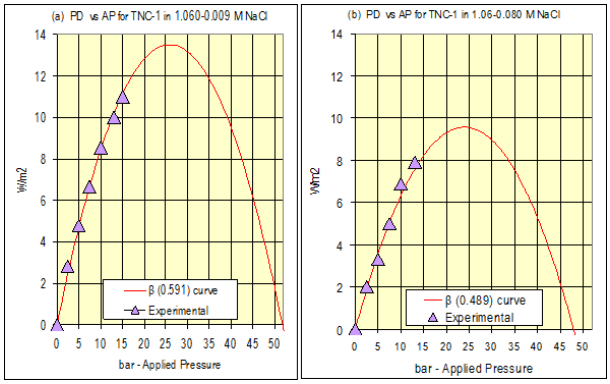

Fig. 12. Maximum PD β projections for TNC-1 at δ > 40 in 1.060–0.009 (a) and 1.060–0.080 (b) M NaCl compared with reported [39] experimental results.

results do not reflect the actual NEPD generation expected of PRO systems under ordinary operation conditions, a subject matter to be discussed in further details elsewhere in this article.

In contrast to the data in Table 1 for advanced PRO TFC membranes, very little information has been made available

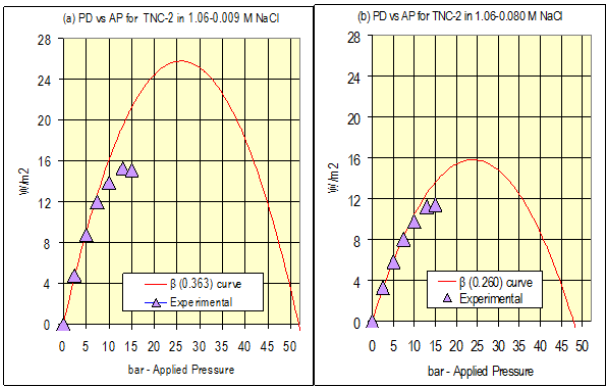

Fig. 13. Maximum PD β projections for TNC-2 at δ > 40 in 1.060–0.009 (a) and 1.060–0.080 (b) M NaCl compared with reported [39] experimental results.

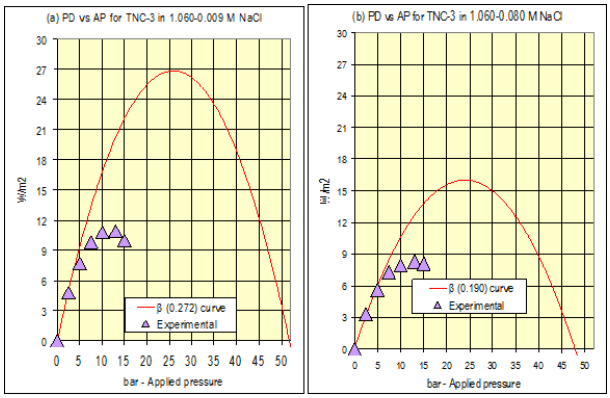

Fig. 14. Maximum PD β projections for TNC-3 at δ > 40 in 1.060–0.009 (a) and 1.060–0.080 (b) M NaCl compared with reported [39] experimental results.

thus far on the behaviors of ordinary RO and FO membranes under PRO conditions. A noteworthy PRO experimental study of an ordinary membrane was reported by Kim and Elimelech [39] on a commercial cellulose triacetate (CTA) FO membrane [41] in the 1.0–0.5; 1.5–0.5; and 2.0–0.5 M NaCl salinity gradients, which simulate osmotic power generation prospects when seawater is paired with brines from current SWRO and future FO desalination plants. The reported [40] experimental PRO flux data for this membrane (A = 0.36 LMH/bar and B = 0.32 LMH) in cited salinity gradients were analyzed in the context of the A–β method as follows. PRO flux at zero AP, the same as FO flux, combined with the permeability coefficient (A) of the membrane were used to determine the FO actual/ideal flux ratio (β) per each salinity gradient, and these terms used for the generation of flux dependent curves on APs wherefrom maximum PD β projection curves were derived and compared with reported experimental results. Ideal and actual PD_{max} curves for CTA are displayed in Figs. 15(a)–(c) for the 1.0–0.5 M NaCl (a); 1.5–0.5 M NaCl (b); and 2.0–0.5 M NaCl (c) salinity gradients. Experimental data points are also provided next to the β projections in Figs. 15(a)–(c). PD_{max} β simulated peaks and their APs (in parentheses) in Figs. 15(a)–(c) are found at 1.17 (12)

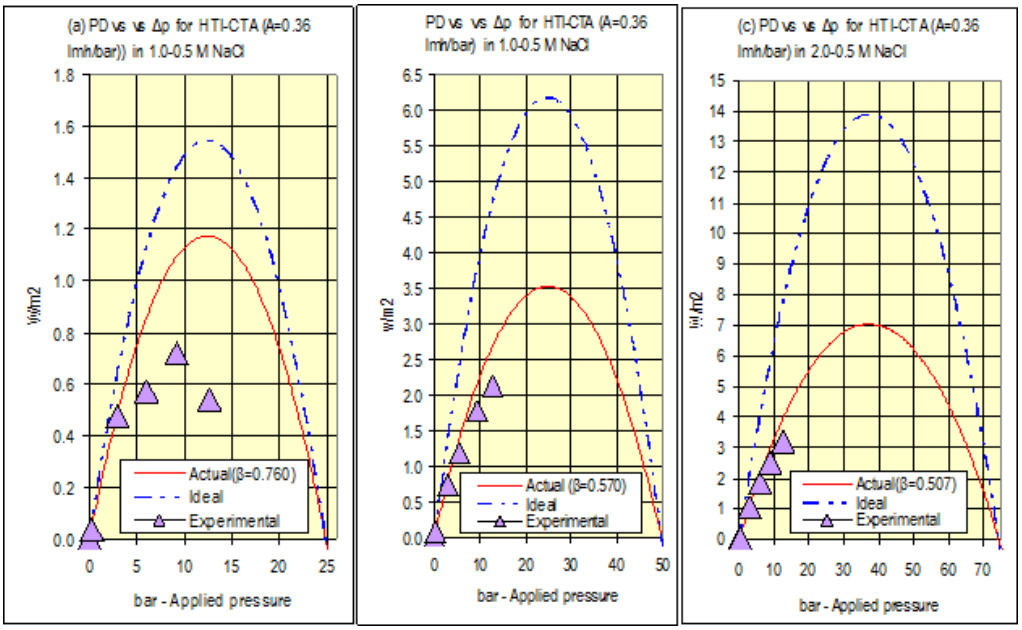

Fig. 15. Ideal and actual PD β projection curves for CTA (A = 0.36 LMH/bar and B = 0.32 LMH) at δ > 40 in 1.0–0.5 M NaCl (a); 1.5–0.5 M NaCl (b); and 2.0–0.5 M NaCl (c) according to the A–β method with experimental data based on flux reported by Kim et al. [40].

for (a); 3.5 (25) for (b); and 7.0 W/m² (35 bar) for (c) as compared with the rigorously simulated respective data of 5.4 (12); 9.6 (23); and 11.1 W/m² (35 bar) in the original report [40]. It should however be pointed out that the reported rigorous model projections make use of A = 1.23 LMH/bar and B = 2.62 LMH, which are said to take into account the membrane's deformation [40], and this explains their higher PD_{max} peaks compared with the respective β projection values. Both the A–β and rigorous methods generate PD curves of similar correlation to the experimental results, which depart significantly in case of the 1.0–0.5 M NaCl salinity gradient with increased agreement by moving to higher HSF ("draw") concentrations. From the results displayed in Fig. 15(a), it could be clearly seen that the experimental PD_{max} peak for 1.0–0.5 M NaCl of ~0.75 W/m² at ~9 bar with A = 0.36 LMH/bar is 36% lower (1.17 W/m²) and appears at a 25% lower pressure (12 bar) compared with the A–β projections (in parentheses). Experimental results of the other CTA projections in Figs. 15(b) and (c) are not available in the vicinity of the peak power; however, the patterns of the curves do suggest actual peaks lower than projections. The β projection curves appear realistic since CTA is known as an inferior PRO membrane compared with advanced TFC membranes, and this is manifested by the results displayed in Figs. 15(a)–(c).

The dependence of β on the salinity gradient at module inlet for the CTA membrane displayed in Fig. 16 according to the data in Figs. 15(a)–(c) shows declined β with increasing salinity gradient, a trend already revealed in Figs. 6(a) and (b) for the TFC membranes HTI and PA-PES. This β trend is true for PRO membranes in general irrespective of type (ordinary and/or TFC). The β values of the CTA ordinary membrane are exceptionally high (0.507–0.760) compared with those cited in Table 1 for TFC membranes, suggesting that ordinary RO and/or FO membranes of higher permeability coefficients (A > 0.36 LMH/bar) could be effective for PRO applications.

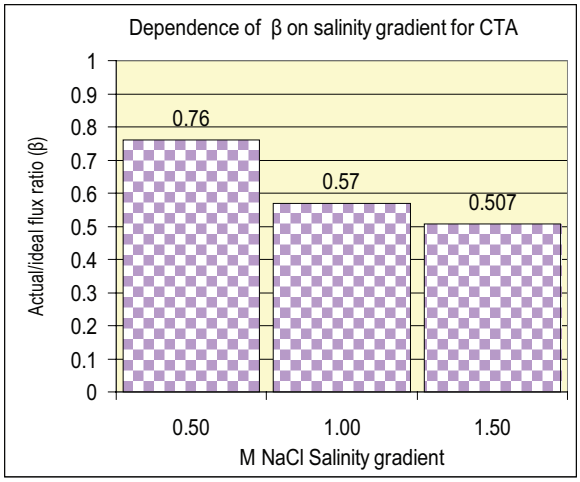

Fig. 16. Actual/ideal flux ratio (β) dependence on feed salinity gradient at the PRO module inlet expressed in M NaCl for the CTA membrane (A = 0.36 LMH/bar and B = 0.32 LMH) for the 1.0–0.5, 1.5–0.5, and 2.0–0.5 M NaCl salinity gradients.

4. Power generation prospects of PRO Systems

According to the A–β method, PRO power generation is a function of A, actual/ideal flux ratio (β), salinity gradient at module inlet, flow ratio (δ) that defines the salinity gradient at module's outlet, and the AP (p_{ap}) of operation. Translation of the salinity gradient average along the module (inlet to outlet) to an average osmotic pressure difference ($\Delta\pi_{av}$) and the knowledge of p_{ap} lead to the average actual flux according to Eq. (2) and to the average PD of the module according to Eq. (3). The agreement between experimental PD results from small lab-bench systems under high

"draw"/permeation flow ratio (δ > 40) conditions and the simulated results by the *A*–β method under such demonstrates the significance of δ in PRO power generation processes. The flow ratio term δ defines the stationary-state conditions inside the PRO module, and fixed δ implies PRO operation with unchanged concentrations at module inlet and outlet of same power prospects. Peak PD under high flow ratio conditions (δ > 40) of little change between the HSD and HSDF concentrations expresses maximum PD availability per given membrane of little, if any, real power output expressed by NEPD. The flow ratio term δ is connected to the percentage permeate in HSDF (α) at module outlet expressed by Eq. (9) with higher δ leading to lower α and vice versa. Since PRO is a single-pass technology, a greater utility of the HSF ("draw") is associated with higher α of lower δ under conditions of less than maximum PD availability. Moreover, maximum PD operation of high δ and low α is associated with high power demand by the auxiliary pumps in the PRO system and, therefore, confines the NEPD output availability of the system. Accordingly, δ is an essential parameter for PRO process optimization to enable maximum NEPD output and this irrespective of the PRO method, conventional or CC-PRO, and their respective apparatus displayed in Figs. 1 and 2.

$$\alpha = 100/(\delta + 1) \tag{9}$$

In light of the aforementioned and since PRO is a single-pass technology of HSF and LSF, the power aspects of a PRO system can be viewed at several levels as follows:

- Actual maximum PD: Actual maximum power availability is described by PD β-projection curve of high flow ratio (δ > 40; β < 1.0; α < 2.44) with PD_{max} peak at a defined AP (AP_{max}). Maximum PD curves and their PD_{max} and APs (AP_{max}) peaks are of little practical significance since proceed with excessively high flow rates and large power consumption of auxiliary pumps and, as a result, yield negative net electric power output (NEPO) for the entire PRO system. In simple terms, the experimental PD_{max} results in Table 1, which correspond to high flow ratio conditions are of little if any practical significance since PRO operation under such conditions leads to negative NEPO.
- Ideal maximum PD: Ideal theoretical PD_{max} is derived from the expression β × PD_{max} for β = 1.0 and δ > 40, and reveals an ideal maximum term in the absence of any membranes' detrimental effects on PRO flux.
- Ordinary PD: Ordinary PD curves with their power peaks at defined APs under ordinary flow ratio (δ) conditions manifest PRO operations of positive NEPD and NEPO of real electric power output to clients.
- NEPD: NEPD stands for ordinary PD less the specific power consumption of the auxiliary components (pumps, turbine-generator, etc.) in the PRO system.
- Maximum NEPD: Maximum NEPD ($NEPD_{max}$) is δ-dependent and expresses the highest PRO NEPO of a given membrane with known β in a defined salinity gradient.

The various power generation aspects of PRO systems are illustrated next in the context of the seawater brine and river water like salinity gradient (SWB-RW) with the best presently reported membrane for such an application. The choice of the SWB-RW illustrated example is no coincidence in light of the growing interest in such an application for energy generation from SWB and TDE. The data in Table 1 of relevance for SWB-TDE PRO applications are found in the salinity gradient range 0.75→1.06 M NaCl HSF concentrations.

5. PRO power generation illustration with the SWB-RW gradient

Among the listed membranes in Table 1, the PES-*B* membrane by Zhang and Chung [37] displays the highest projected β (0.447) curve (Fig. 10(b)) with peak (PD_{max}) of 23 W/m² (24 bar) experienced with δ = 40 for the 1.00 M NaCl salinity gradient, typical of SWB-RW like gradients of worldwide abundance. Compared with PES-*B*, the PES-*A* membrane [38] under the same conditions displays (Fig. 10(a)) only slightly inferior performance characteristics. The application of the CC-PRO simulation database [21–24] to the PES-*B* membrane (*A* = 3.3 LMH/bar; β = 0.447) in the 1.00–0.01 M NaCl (5.820%–0.058% NaCl) salinity gradient under flow ratio conditions of δ = 40 (Q_{HSF}/Q_p) and Q_{LSC}/Q_{LSF} = 0.15 (85% permeate recovery from LSF) is illustrated in Table 2 and reveals PD_{max} = 21.8 W/m² (24 bar) associated with NEPD = –31.8 W/m² and NEPO = –6.35 kW per module of 200 m² membrane surface area. As expected, PD_{max} in this case is somewhat lower compared with that in Fig. 10(b) (~21.8 W/m² instead of ~23.0 W/m²) since the salinity of the LSF solution is somewhat higher (0.058% instead of 0.000%). Plugging the essential parameters of the feed solutions concentrations and their osmotic pressures; *A*; β; δ (Q_{HSF}/Q_p); Q_{LSC}/Q_{LSF} flow ratio; and efficiencies of auxiliary pumps and turbine-generator into the PRO database program displayed in Table 2 leads automatically to complete PD and NEPD β-projection curves as function of AP. Specific PD and NEPD values for a selected AP are displayed in the main frame of the program when the selected pressure is plugged into the database and the average actual flux display in the bottom right-hand side of the table is adjusted. The ideal (β = 1.00), actual (β = 0.447) PD, and NEPD simulated CC-PRO curves for said gradient system at δ = 40 are illustrated in Fig. 17.

Change of δ in the CC-PRO simulation database (Table 2) automatically generates completely new power curves, and such PD curves in the context of the salinity gradient under review are illustrated in Fig. 18 for the PES-*B* membrane with δ of 0.75 (57.1%), 1.0 (50%). 2.0 (33.3%), 3.0 (25%), 5.0 (16.7%), 10.0 (9.1%) and 40.0 (2.4%), wherein the data in parentheses pertain to α (percentage permeate in HSDF). Analogous data are furnished in Fig. 19 in reference to NEPD. The trend of declined PD peak and its AP with decreased δ is clearly evident in Fig. 18. The trend with regard to NEPD displayed in Fig. 19 is more complex and reveals NEPD increase with decline of δ (40.0→3.0) displayed in Fig. 20(b), maximum NEPD at δ = 3.0, and NEPD decrease with a further decline of δ (3.0→0.75) displayed in Fig. 20(a). The NEPD shifts with δ are also accompanied with peak power AP shifts of 33 (δ = 10.0); 29 (δ = 5.0); and 26 (δ = 3.0) bar displayed in Fig. 20(b) and 26 (δ = 3.0); 24 (δ = 2.0); 21 (δ = 1.0); and 20 (δ = 0.75) bar displayed in Fig. 20(a). The information disclosed in Fig. 20 for the PRO system under review reveals maximum NEPD

Table 2
CC-PRO power simulation database for the PES-*B* membrane (*A* = 3.3 LMH/bar and β = 0.447) in the 5.820%–0.058% NaCl) salinity gradient under flow ratio conditions of $Q_{HSF}/Q_p(\delta) = 40$ and $Q_{LSC}/Q_{LSF} = 0.15$ (85% permeate recovery from LSF)

5.820	% NaCl - HSF	48.6 bar π
0.058	% NaCl - LSF	0.5 bar π
25	°C	48.1 bar Δπ

Design & Membrane Data

1	Number of Modules
1	No of Membrans per Module
205	cm length of module
30	cm, inner diameter of module
145	liter, gross volume of module
50.0	% membrane volume in module*
72.4	liter net volume of Module
200.0	m2, membrane surface per module
200.0	m2 total surface area of design

LSF-LSC Performance Data

Module	Unit	
8.05	8.05	m3/h LSF Inlet Flow
0.06	0.06	% LSF inlet Salinity
1.21	1.21	m3/h LSC outlet Flow
0.39	0.39	% LSC outlet Salinity
6.84	6.84	m3/h Permeation Flow
0.22	0.22	% mean Salinity (inlet+outlet)/2
1.86	1.86	bar mean Δπ (inlet+outlet)/2
0.15	0.15	Ratio Q_{LSC}/Q_{LSF} $Q_p=Q_{LSF}-Q_{LSC}$
85	85	% permeate recovery from LSF

8.35 Δπ(bar)/C(%) - van't Hoff conversion constant

PRO Membranes Detrimental Effect

0.447	Ratio Actual/Ideal
55.3	% Detrimental Effects

Fixed Flux per Single Module

34.2	LMH, Flux (Selected average)
6.84	m3/h (Q_p) Module average Permeate
114	lpm Module average Permeate

Recycled Flow (CP) of Single Module

273.6	m3/h recycling flow (Q_{CP})
4560	lpm recycling flow (Q_{CP})
0.02	minute complete volume recycle
40.00	Selected Flow Ratio (Q_{CP}/Q_p)
0.016	min., HSF residence in module

Flow of Entire Design

6.84	m3/h Permeate Flow of entire unit
273.6	m3/h Recycling Flow of entire unit
2.44	% permeate in HSDF

HSF - HSDF Module Inlet & Outlet Data

5.8	% HSF Module Inlet
48.1	bar Δπ Module Inlet
5.7	% HSDF Module Outlet
-3.2	bar Δπ Module Outlet
5.7	% HSDF average
22.5	bar Δπ Module average

Power Demand of CC-PRO PUMPS

Performance	HSP	LSP	CP
m3/h	273.6	8.05	**273.6**
bar*	0.50	0.50	0.50
Efficiency*	0.75	0.75	0.75
Power (w)	5067	149	5067

TOTAL-Pumps Power Demand (w)	**10,282**
TOTAL-Pumps Power Density (W/m2)	51.4
Actual PRO of membrane (W/m2)	**21.8**
Pumps Demand (W/m2)	-51.4
Turbine-Generator-10% PRO loss	-2.2
Net Electric Power (w/m2)	**-31.8**
Net Electric Power Output of Unit (kW)	**-6.35**
Energy per m3 Permeation (kWh/m3)	-0.929
Energy per m3 LSF (kWh/m3)	-0.789
Energy per m3 HSF (kWh/m3)	-0.023

PRESSURE, NDP and FLUX DATA

Permeability Coefficient (l/m2/h/bar)				3.30
Module Parameters		Ideal		Actual
Type	bar	NDP	FLUX	FLUX
Applied Pressure	23.0	bar	LMH	LMH
Δπ MOD Inlet	48.1	25	83	37
Δπ MOD Outlet	44.2	21	70	31
Δπ MOD average	46.2	23.2	76.5	34.2
CC-PRO Selected average Flux				34.2

* **Assumed**

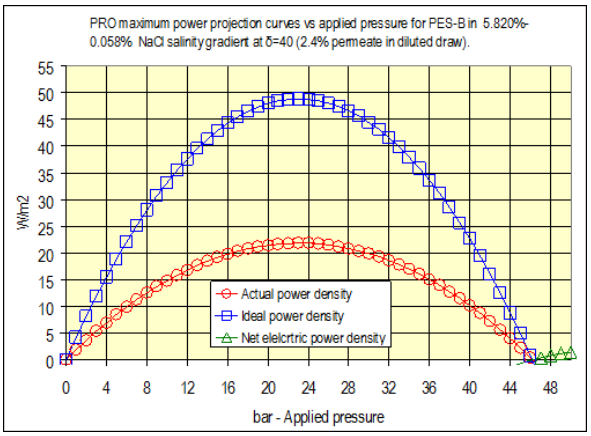

Fig. 17. CC-PRO simulated maximum actual and ideal PD β projection curves as function of applied pressure according to the database in Table 2 for PES-*B* at δ = 40, which defines the stationary-state conditions inside the PRO module at near maximum PD availability.

availability of ~10.0 W/m² (26 bar) with δ = 3.0; a somewhat lower NEPD value of 9.5 W/m² (24 bar) with δ = 2.0; and 8.0 W/m² (21 bar) with δ = 1.0. The summary of the simulated PD and NEPD β projections with δ = 3.0 in Fig. 21 shows ideal PD of ~40 W/m² at 21 bar, actual PD of ~18 W/m² at 21 bar, and an ultimate maximum NEPD of ~10 W/m² at 26 bar. Likewise, β-projection summary with δ = 1.0 in Fig. 22 shows ideal PD of ~30 W/m² at 18 bar, actual PD of ~14 W/m² at 18 bar, and an ultimate maximum NEPD of ~7.0 W/m² at 22 bar.

The aforementioned PD and NEPD projections by the *A*–β method for PES-*B*, the presently best available membrane for SWB-RW like salinity gradient applications, reveal the realistic prospects for power generation from such systems in the context of the CC-PRO technology of near absolute energy conversion efficiency. The projected data show that PD and NEPD are two different terms with the latter manifesting the actual PRO electric power sold to customers, a parameter of clear economic significance. In the system under review, maximum NEPD availability of ~10 W/m² (2.0 kW NEPO per module of 200 m² membrane's surface area) takes place with δ = 3.0. Said maximum according to Fig. 21 represents ~25% of the ideal maximum PD (40 W/m² for β = 1.00 at 21 bar) and ~55.5% of the actual PD peak power (18 W/m² for β = 0.447 at 21 bar). The PRO performance at δ = 1.0 (α = 50%) in Fig. 22 compared with that of δ = 3.0 (α = 25%) in Fig. 21 is characterized by declined power availability with shift of power peaks to lower APs. Another noteworthy feature in these figures is the appearance of the NEPD peak at higher AP compared with that of the PD peak.

The power projections considered hereinabove for the PES-*B* membrane for the SWB-RW like salinity gradient are in the context of the CC-PRO technology of near absolute energy conversion efficiency without need of ERD. Accordingly, the application of conventional PRO with ERD instead of CC-PRO is expected to yield lower PD and NEPD projections as result of energy losses associated with the ERD. Since PES-*B* is the membrane of the highest β value (0.447) among the advanced TFC membranes cited in Table 1 for salinity gradients around 1.0 M NaCl, the projected CC-RO power performance of this membrane disclosed the present state-of-the-art for power generation from SWB-RW like salinity gradients.

6. Discussion – principal aspects of PRO

The ultimate development of the conventional PRO for commercial hydroelectric power generation applications should relate to the technology aspects and in particular to the performance of the membranes and ERD. In light of the recently reported [20] CC-PRO technology of near absolute energy conversion efficiency without need for ERD, the conventional technology constrains have been lifted including the need for better ERD. Accordingly, the membrane aspects of PRO are at present time the single most important issue in the development of commercially viable PRO applications, a subject matter considered hereinafter.

6.1. PRO membranes development priority

According to the collective data in Table 1, PRO PD peaks show near linear dependence on salinity gradients (Fig. 5(c)) and peak APs (Fig. 5(b)) and exponential dependence on β (Fig. 5(a)). The exponential dependence of β on the salinity gradient is also evident in Fig. 6 for the same TFC membranes and in Fig. 16 for the conventional CTA membrane. The aforementioned rules out the prospects for universal PRO membranes and advocates focus on the development of PRO membranes for specific applications in defined salinity ranges. Noteworthy specific applications as presently viewed include hydroelectric power generation from gradients like SW-RW (0.5 M NaCl); SWB-RW (1.0 M NaCl); SWB-SW (0.5 M NaCl); and SWC-SW and SWC-SWB (>1.5 M NaCl); wherein the data in parenthesis are of typical M NaCl equivalents and the seawater-related terminology, SW, SWB, and SWC, distinguishes between seawater, brine from seawater desalination plants, and seawater concentrates derived from evaporation ponds. The SW-RW and SWB-RW salinity gradients also cover the subsection SW-TDE and SWB-TDE where TDEs apply instead of river water (RW).

The highest priority in the development of PRO membranes should be directed toward SW-RW like salinity gradient applications, which are of the greatest worldwide prospects. Newly developed membranes for SW-RW and/or SW-TDE applications should possess *A* > 2.5 LMH/bar; β > 0.7; and mechanical strength to withstand APs of 15–17 bar. The MP#1 (*A* = 5.81 LMH/bar; *B* = 0.88 LMH; *S* = 349 μm) by Yip et al. [34] with β = 0.374 of PD_{max} = 10 W/m² and $NEPD_{max}$ = 4.2 W/m² [21,22] is the best reported membrane for SW-RW applications at present time, and newly developed advanced membranes of cited *A* (>2.5 LMH/bar) and β (>0.7) parameters should enable the attainment of NEPD > 7.0 W/m², thereby, making this PRO application economically viable in the context of the CC-PRO technology for large-scale worldwide operations.

The next highest priority in the development of advanced PRO membranes should focus on the SWC-SW and SWC-SWB (>1.0 M NaCl) salinity gradients, since SWC from evaporation ponds in the vicinity of seashore lines and/or from FO processes may apply to large-scale clean power generation in many worldwide regions of suitable arid zone climate

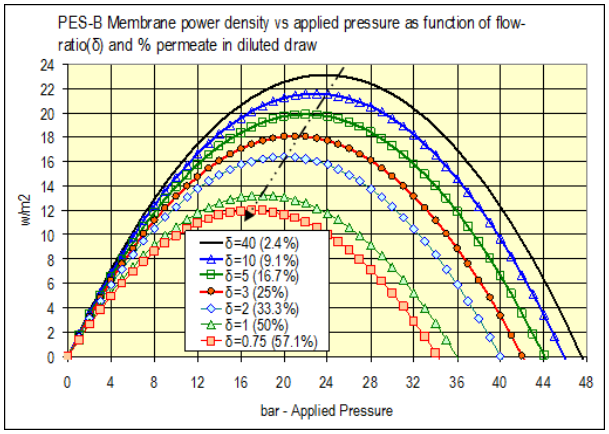

Fig. 18. CC-PRO PD β projection curves for PES-*B* according to the database in Table 2 as function of applied pressure and flow ratio (δ), which defines the stationary-state conditions inside the PRO module.

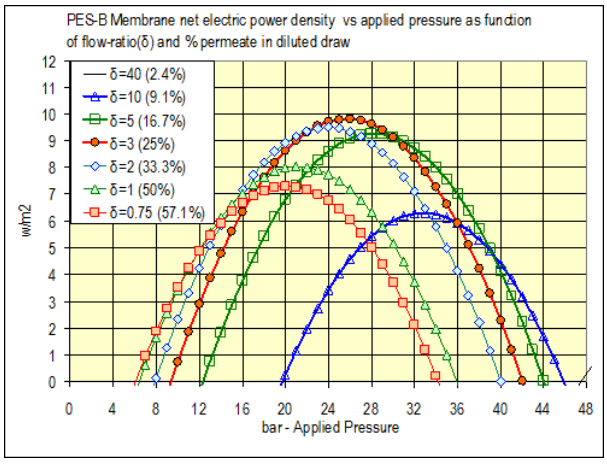

Fig. 19. CC-PRO NEPD β projection curves for PES-*B* according to the database in Table 2 as function applied pressure and flow ratio (δ), which defines the stationary-state conditions inside the PRO module.

for such applications. Development of membranes for such applications should focus on attainment of high mechanical strength to withstand high APs (>45 bar) of cited salinity gradients. The HTI-TFC membrane (*A* = 2.49 LMH/bar; *B* = 0.39 LMH; *S* = 564 μm) studied by Straub et al. [35] is the best reported membrane for SWC-SW applications at present time with a demonstrated 700 psi (48.3 bar) limit of AP. The evaluation the power generation prospects of this HTI-TFC membrane in context of CC-PRO for the Dead Sea (DS) and Red Sea brine (RSB) salinity gradient (DS [34.0%]–RSB [7.13%]) using β = 0.123 gave a simulated NEPD projection of 23.1 W/m^2 at the 700 psi limit AP [23], suggesting a clear economic feasibility already at this stage. It should be pointed out that the PRO power generation from the cited DS (34.0%)–RSB (7.13%) salinity gradient is of concrete significance in light of the Jordanian RS to DS water transfer program, which also includes RS water desalination with RSB

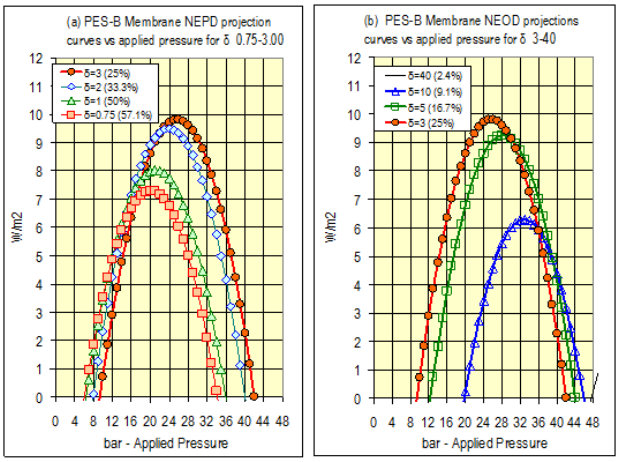

Fig. 20. CC-PRO NEPD β projection curves for PES-*B* according to the database in Table 2 as function of applied pressure and flow ratio (δ), which defines the stationary-state conditions inside the PRO module showing maximum power and its decrease (a) and increase (b) as function of δ.

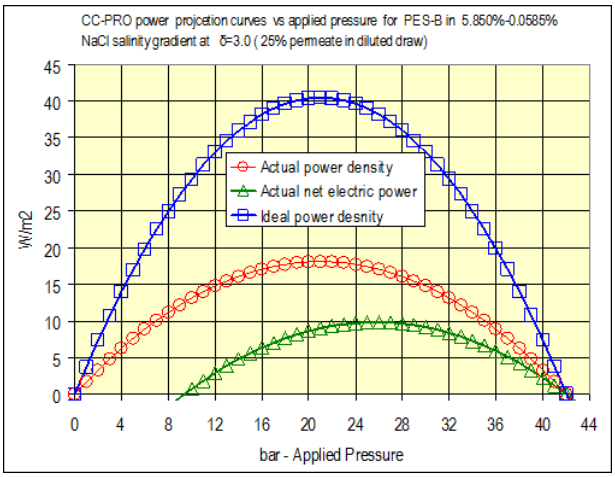

Fig. 21. CC-PRO simulated ideal and actual power β projection curves as function of applied pressure according to the database in Table 2 for PES-*B* at δ = 3.0, which defines the stationary-state conditions inside the PRO module.

disposed to the DS. CC-PRO simulation of the same HTI-TFC membrane with the SWC (25%)–SW (4.2%) salinity gradient using β = 0.191 gave NEPD of 39.3 W/m^2 under the AP limit of 700 psi [24], suggesting a clear economic feasibility already at this stage of even greater prospects compared with the previous example. The principal objectives in the development of viable PRO membranes for high salinity gradients applications should include the attainment of high mechanical strength to enable high AP limits (>700 psi); *A* > 2.5 LMH/bar, and β > 0.200. Newly fabricated membranes for higher operational pressures (>700 psi) of greater *A* (>2.5 LMH/bar) and β (>0.200) are expected to become available in the near future, making the above-referred CC-PRO applications even more cost effective.

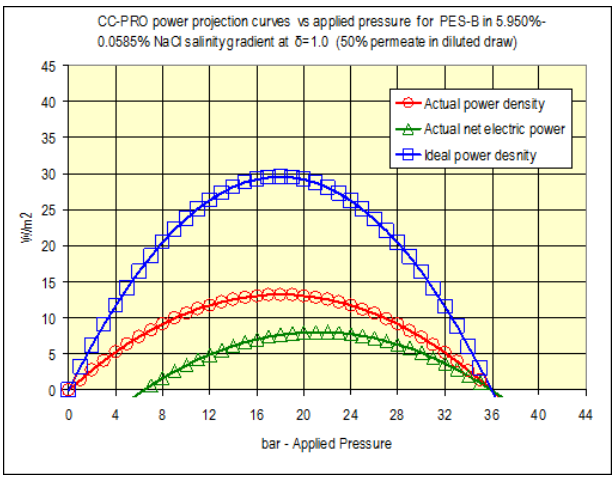

Fig. 22. CC-PRO simulated ideal and actual power β projection curves as function of applied pressure according to the database in Table 2 for PES-*B* at δ = 1.0 (α = 50%), which defines the stationary-state conditions inside the PRO module.

The most extensively investigated PRO membranes at present time relate to the salinity gradient range 0.75–1.10 M NaCl in conjunction with SWB-RW as a model for the energy recovery prospects from SWB-TDE systems. The increased awareness of this PRO application was stimulated by the "Mega-ton Water System" project in Japan [28–30]. According to Table 1, the PES-*B* membrane (*A* = 3.3 LMH/bar and β = 0.447) by Zhang and Chung [37] reveals the best performance characteristics in the salinity range under review, and its detailed performance analysis for the SWB (5.820%)-RW (0.058%) salinity gradient is summarized in Fig. 21 and shows maximum NEPD of ~10 W/m^2 with β = 0.447 at δ = 3.0 (25% permeate in HSDF). This maximum is associated with specific energy (SE) of 0.334 kWh/m^3 for the LSF, which implies the need for ~ 9.0 m^3 of RW, or a greater volume of TDE, in order to generate enough PRO energy for the desalination of 1.0 m^3 of seawater (3.0 kWh/m^3). In simple terms, the use of PRO SWB-TDE generated energy to supplement the power needs of SWRO is of minor significance and highly ineffective, especially since high recovery low-energy desalination of TDE was already demonstrated on large commercial scale in Orange District, California, USA [42], and by PUB in Singapore [43] as well as at the pilot level in the Safdan Center, Israel [56], and by LA Sanitation, USA [57].

The PES-*B* membrane by Zhang and Chung [37] represents the current state-of-the-art performance for SWB-RW like applications, and further improvements of membrane for such applications should account for *A* > 3.3 LMH/bar, β > 0.447, and mechanical strength to withstand pressure up to 27 bar.

6.2. A simple scanning procedure of newly fabricated PRO membranes

The enormous worldwide effort to develop new effective PRO membranes covers both intricate fabrication and characterization techniques. The genuine need for quick and simple scanning procedures to assess the performance of newly fabricated PRO membranes is evident and obvious since could save both time and costs in the early stage and enable to conduct extensive investigations only on promising membranes. The *A*–β method described hereinabove for many of the recently reported advanced PRO membranes is an ideal scanning procedure since provides instant projections of flux, PD and NEPD curves as function of AP per given salinity gradient by the knowledge of the permeability coefficient (*A*) and the FO actual/ideal flux ratio (β) parameters, both readily available soon after the fabrication of a new PRO membrane for a specific application. The present study shows the close resemblance between the flux and PD_{max} projection curves of the *A*–β and rigorous methods and their consistency with experimental results, and this implies that the *A*–β method is trustworthy. Moreover, the *A*–β method also provide knowledge of NEPD availability as function of flow ratio (δ) under actual PRO operational conditions, including the optimized maximum NEPD, which is an important parameter for the economic assessment of newly fabricated membranes for their designated applications. Accordingly, the adaptation of the *A*–β scanning method of newly fabricated PRO membranes as a standard procedure could greatly assist researchers in this area and enhance their productivity. The *A*–β scanning method will enable to focus mainly on promising PRO by ignoring membranes of poor initial scan results.

6.3. Real PRO power availability of membranes

The increased numbers of publications pertaining to the fabrication and/or performance evaluation of new PRO membranes provide rigorous model calculations of flux and PD curves together with experimental results to validate the theoretical projections. Unfortunately, most of the published PRO experimental data originate from small lab-bench systems under high flow ratio (δ > 40) conditions, which are frequently operated also by recycled HSF and LSF solutions with continuously changing stationary-state conditions inside the PRO module. Experimental data generated under such experimental conditions with little difference between inlet and outlet module concentrations and osmotic pressures correspond to high flux conditions of maximum PD projections with little practical significance since PRO is a single-pass process and expected to proceed at a much lower flow ratio (δ: 1–5 instead of 40 or more) with a much higher percentage permeates in the HSDF (α: 20%→50% at δ: 5→1 instead of α < 2.44% at δ > 40). In simple terms, the experimental flux and PD_{max} at high flow ratio (δ) from small lab-bench systems are far removed from the actual PRO operational parameters and ignore the issue of NEPD, the single most important parameter of the PRO technology, which takes into account the power consumption of the auxiliary pumps in the PRO system without which it could not be operated. While the reported flux and PD_{max} experimental results from small lab-bench systems are trustworthy and indicative of the membrane performance, they create the illusion of high PD expectation from PRO systems since ignore the optimized PD as function of flow ratio (δ) and, more importantly, ignore the optimized NEPD as function of δ, which is the most important parameter of the PRO technology. The adaptation of the *A*–β method for the performance assessment of newly fabricated PRO membranes provides a powerful tool in the hands of researchers to generate realistic

power projection of membranes under normal PRO operational conditions right from start.

6.4. Conventional and closed-circuit PRO techniques

Conventional PRO with ERD in its center (Fig. 1) wherein pressure exchange takes place between the same flow rates of discharged pressurized HSDF and the HSF supply. The PRO AP of operation is preserved by the ERD and modified by the BP to supplement for the pressure losses encounter in the pressure exchanger device. In the case of CC-PRO (Fig. 2), no ERD is requires, and the PRO AP is part of the intrinsically created osmotic pressure inside the module, which dictates the desired average flux formation (J_{av}) according to Eq. (2). CC-PRO is a technique of near absolute energy conversion efficiency with negligible energy losses encountered only during the hydrostatic compression/decompression of the SC. The energy recovery efficiency aspects in the two conventional PRO demonstration units with PX-ERD, which operated in Norway [25–27] and Japan [28–30], have never been disclosed to allow the assessment experimental results with regard to the ERD efficiency in PRO systems. Avoiding the need for ERD in PRO by the use of the CC-PRO technology of near absolute energy conversion efficiency makes it the method of choice for future PRO operations in light higher expected power output and lower installation costs of increased cost effectiveness.

6.5. Standalone PRO and its hybrids

PRO is a standalone membrane technology for hydroelectric power generation from salinity gradients, which looks deceptively simple at first despite its inherent complexity as already discussed hereinabove. The making of this technology self-sustained with ideal HSF ("draw") and LSF ("feed") feed solutions requires their recycling, and various hybrid systems for "draw" recycling were proposed on the basis of RO, membrane distillation (MD), thermal dissociation, and water separation by means of hydrogel or magnetic particles. A typical CC-PRO hybrid system for autonomous operation with feed solutions (HSF and LSF) recycling RO means is displayed in Fig. 23(A) with emphasis on flow rates. The HSF recycling process proceeds with RO permeate flow (Q_p) separation from the combined flow of HSDF (Q_{HSDF}) in the draw recycling unit (DRU), wherefrom the flow of brine is the restored HSF (Q_{HSF}) and the flow of permeate (Q_p) after blending with the LSC (Q_{LSC}) is the restored LSF (Q_{LSF}). The PRO section in the hybrid generates power (P_{PRO}) whereas that of the DRU consumes power (P_{DRU}) and net power output from this self-sustained system is the difference between them ($P_{PRO} - P_{DRU}$). Power output from the hybrid system displayed in Fig. 23(A) is a thermodynamically unfavorable process even when the membrane performs ideally ($\beta = 1.0$), and DRU takes place by means of RO, the method of the highest entropy efficiency available today [44], since the mixing energy made available through PRO is insufficient to cover the separation energy requirements of RO.

Another hybrid approach is illustrated in Fig. 23(B) for electric power generation from a waste heat source through PRO. This scheme could be valid pending high energy conversion efficiency of PRO, low installation costs, and operational expenses arising from the DRU, and demonstrated cost effectiveness for the entire system compared with other techniques such as the Rankine Cycle [45] for electric power generation from waste heat sources. The cited constrains with regard to the Fig. 23(A) design also apply to the Fig. 23(B) hybrid configuration, suggesting that such PRO hybrid technologies are not sufficiently mature at present time.

A noteworthy 35M$ program in Korea named GMVP (G for global; M for membrane distillation; V for valuable resources recovery; and P for PRO) intends to install a 1,000 m^3/d SWRO pilot, a 400 m^3/d MD pilot, and a 200 m^3/d PRO pilot and through hybridization of RO and MD with PRO enabled to reduce the volume of disposed brine after the recovery of valuable ingredients (e.g., Li) as well as reduce the SWRO desalination energy [46]. The reported overview scheme of this program in Fig. 24(A) identifies the SWRO-PX and PRO-PX technologies to be explored and, however, does not reveal the mode of integration of MD in the hybrid system. This program should provide valuable information about the role of PX in conventional SWRO and PRO processes, since PX is a key element in the design. The PX steps are intended for pressure boosting of SW feed at inlet to HP and, thereby, reduce the overall energy need for SW desalination by utilizing both TDE and SWB through PRO. While important, the GMVP program is not based on state-of-the-art technologies such as SWRO-CCD [32,47–55] and CC-PRO [19–24], which operate with near absolute energy conversion efficiency without need of PX-ERD. Moreover, the PRO application of the SWB-TDE salinity gradient in conjunction with SWRO desalination is an ineffective approach, since TDE is a valuable source for high recovery and low-energy direct production of freshwater already practiced on large scale in Orange District, California, USA [42] and by PUB in Singapore [43]. An alternative design that complies with the objectives of the GMVP program on the basis of advanced closed-circuit technologies is displayed in Fig. 24(B); wherein, reduction in seawater desalination energy consumption proceeds by means of the CCD-SWRO with power supplement created by CC-PRO electric power generation from the SWB-TDE salinity gradient. In this instance, the consecutive sequential CCD process under fixed flow and variable pressure conditions was already demonstrated to proceed with SW desalination of 50% recovery under 1.7 kWh/m^3 [55] without need for ERD, and such a low energy is unattainable by conventional SWRO-PX techniques according to the hybrid design displayed in Fig. 24(A). Moreover, if part of the energy needs of

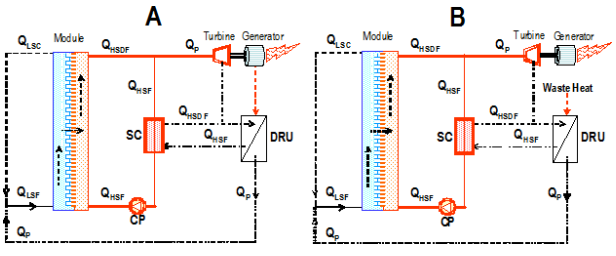

Fig. 23. Schematic illustration of CC-PRO hybrid systems with draw recycling units (DRU) for autonomous operation (A) and for conversion of waste heat to electric power through PRO (B).

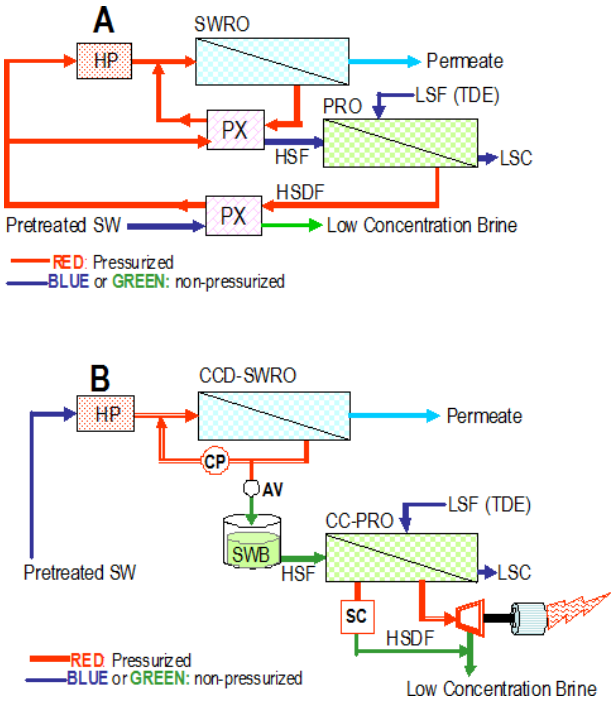

Fig. 24. The proposed [46] flow diagram of the SWRO-PRO hybrid system of the GMVP Korean program (A) and its SWRO-CCD and CC-PRO equivalent (B).
Note: Abbreviations are the same as defined elsewhere in this article.

the CCD-SWRO process shall be supplied by CC-PRO power generation using the SWB-TDE salinity gradient system according to the design in Fig. 24(B), this should enable a further drop of the desalination energy under 1.4 kWh/m^3. For reasons already specified hereinabove, both hybrid designs in Figs. 24(A) and (B) are not recommended for commercial applications.

7. Concluding remarks

The present study analyses the performance of advanced PRO membranes in the context of the CC-PRO, a technology of near absolute energy conversion efficiency without ERD with emphasis made regarding the present state-of-the-art of the various aspects. A meaningful PRO future progress requires the identification of genuine needs and establishing priority regarding desired performance characteristic of membranes in the context of salinity gradients of high prospects for commercial applications. Priorities suggested by the present study in the context of CC-PRO technology are as follows:

- Need to develop simple, quick, and reliable performance evaluation techniques for PRO membranes for which the A–β method is proposed and recommended.
- Need to develop simple, quick, and reliable techniques for NEPD projections, the most important parameter of PRO for which CC-PRO simulations are proposed and recommended.
- Need to development reliable bench-scale apparatus for single-pass PRO flux measurements as function of flow ratio (δ), which defines the stationary-state condition inside the PRO module.
- Preference of CC-PRO without ERD instead of convention PRO with ERD for higher (25%–40%) power output.
- Emphasis on the development of PRO membranes with high β for SW-RW applications, the salinity gradient of the highest global availability and greatest commercial prospects and on membranes with high mechanical strength to withstand APs of salinity gradients comprised SW and its concentrates.

The CC-PRO performance analysis in the present study covers most major advanced PRO TFC type membranes (Table 1; Figs. 3–14) in the forms of flat and/or hollow fiber configuration as well as that of CTA (Figs. 15(a)–(c) for which experimental data were made available. The inclusion of CTA (A = 0.36 LMH/bar and B = 0.32 LMH) arises from the analysis of the recent experimental data by Kim and Elimelech [40] that reveal extraordinarily high β values (Fig. 16) of 0.76 (0.5), 0.57 (1.0), and 0.507 (1.5) as function of the M NaCl salinity gradient (in parentheses). These findings suggest that treated and/or modified cellulose membranes of higher permeability coefficients (A > 0.36 LMH/bar), or alike, could also be found effective for PRO applications, although not of TFC type. The present state of knowledge is insufficient to allow clear statements regarding the preferred configuration (flat vs. hollow fiber) and/or type (TFC vs. ordinary) of the ultimate PRO membranes.

References

[1] S. Loeb, S. Sourirajan, American Chemical Society, Advances in Chemistry Series, Vol. 38, 1963, pp. 117–132.
[2] S. Loeb, Method and Apparatus for Generating Power Utilizing Pressure-Retarded-Osmosis, US Patent No. 3,906,250, 1975.
[3] S. Loeb, Production of energy from concentrated brined by pressure-retarded osmosis, preliminary technical and economic correlations, J. Membr. Sci., 1 (1976) 49–63.
[4] S. Loeb, Osmotic power plants, Science, 189 (1965) 654–655.
[5] S. Loeb, Energy production at the Dead Sea by pressure-retarded osmosis: challenge or chimera? Desalination, 120 (1998) 247–262.
[6] A. Achilli, T.Y. Cath, A.E. Childress, Power generation with pressure retarded osmosis: an experimental and theoretical investigation, J. Membr. Sci., 343 (2009) 42–52.
[7] A. Achilli, T.Y. Cath, A.E. Childress, Selection of inorganic-based draw solutions for forward osmosis applications, J. Membr. Sci., 364 (2010) 233–241.
[8] A. Achilli, A.E. Childress, Pressure retarded osmosis: from the vision of Sidney Loeb to the first prototype installation – review, Desalination, 261 (2010) 205–211.
[9] M. Elimelech, W.A. Phillip, The future of seawater desalination: energy, technology, and the environment, Science, 333 (2011) 712–717.
[10] B.E. Logan, M. Elimelech, Membrane-based processes for sustainable power generation using water, Nature, 488 (2012) 313–319.
[11] S.J. Duraneau, Emergence of forward osmosis and pressure retarded osmosis process for drinking water treatment, Florida Water Resour. J., (2012) 32–36.
[12] X. Wang, Z. Huang, L. Li, S. Huang, E.H. Yu, K. Scott, Energy generation from osmotic pressure difference between the low and high salinity water by pressure retarded osmosis, J. Technol. Innov. Renew. Energy, 1 (2012) 122–130.
[13] T.-S. Chung; X. Li, R.C. Ong, Q. Ge, H. Wang, G. Han, Emerging forward osmosis (FO) technologies and challenges ahead for clean water and clean energy applications, Curr. Opin.Chem. Eng., 1 (2012) 246–257.

[14 L. Checkli, S. Phuntsho, H.K. Shon, S. Vigneswaran, J. Kandasamy, A. Chahan, A review of draw solutes in forward osmosis process and their use in modern applications, Desal. Wat. Treat., 43 (2012) 167–184.
[15] I.L. Alsvik, M.-B. Hägg, Pressure retarded osmosis and forward osmosis membranes, Polymers, 5 (2013) 303–327.
[16] F. Dinger, T. Tröndle, U. Platt, Optimization of the energy output of osmotic power plants, J. Renew. Energy, 2013 (2013) 1–7.
[17] C. Klaysom, T.Y. Cath, T. Depuydt, I.F.J. Vankelecom, Forward and pressure retarded osmosis: potential solutions for global challenges in energy and water supply, Chem. Soc. Rev., 42 (2013) 6959–6989.
[18] M. Sabah, A.F. Atwan, H.B. Mahood, A. Sahrif, Power generation based on pressure retarded osmosis: a design and an optimization study, Int. J. Appl. Eng. Manage., 2 (2013) 68–74.
[19] A. Efraty, Power Generation Pressure Retarded Osmosis in Closed Circuit without Need of Energy Recovery, PCT/IL2012/050135, International Publication Number WO 2012/140659 A1, 2012.
[20] A. Efraty, Pressure-retarded osmosis in closed circuit: a new technology for clean power generation without need of energy recovery, Desal. Wat. Treat., 51 (2013) 7420–7430.
[21] A. Efraty, Closed circuit PRO series no 2: performance projections for PRO membranes by a simple approach base on actual/ideal flux ratio at zero applied pressure, Desal. Wat. Treat., 57 (2016) 6633–6643.
[22] A. Efraty, Closed circuit PRO series no 3: status and prospects for PRO hydroelectric power generation from sea-river water like salinity gradients, Desal. Wat. Treat., 57 (2016) 7131–7148.
[23] A. Efraty, Closed circuit PRO series no 4: CC-PRO hydroelectric power generation prospects from the Red-Sea brine and Dead-Sea salinity gradient, Desal. Wat. Treat., 55 (2015) 1983–1997.
[24] A. Efraty, Closed circuit PRO series no 5: clean energy generation from seawater and its concentrates by CC-PRO without need of energy recovery, Desal. Wat. Treat., 57 (2016) 8035–8049.
[25] S.E. Skilhagen, J.E. Dugstad, R.J. Aaberg, Osmostic power – power production based on the osmotic pressure difference between waters and varying salt gradients, Desalination, 220 (2008) 476–482.
[26] S.E. Skilhagen, G. Brekke, W.K. Nielsen, Progress in the Development of Osmotic Power, Proc. 2011 Qingdao International Conference on Desalination and Water Reuse, Qingdao, China, 2011, pp. 247–260.
[27] G. Brekke, Review of Experience with the Statkraft Prototype Plant, The 3rd Osmosis Membrane Summit, Barcelona, Spain, 2012.
[28] A. Tanioka, Power Generation by Pressure Retarded Osmosis Using Concentrated Brine from Seawater Desalination System and Treated Sewage, Review of Experience with Pilot in Japan, The 3rd Osmosis Membrane Summit, Barcelona, Spain, 2012.
[29] M. Kurihara, Government Funded Programs Worldwide, The Japanese "Mega-ton Water System" Project, The 3rd Osmosis Membrane Summit, Barcelona, Spain, 2012.
[30] K. Saito, M. Irie, S. Zaitsu, H. Sakai, H. Hayashi, A. Tanioka, Retarded osmosis using concentrated brine from SWRO system and treated sewage as pure water, Desal. Wat. Treat., 41 (2012) 114–121.
[31] A. Hermoni, Actual Energy Consumption and Water Cost for the SWRO Systems at Palmachim – Case History, IDA Conference, Huntington Beach, CA, USA, 2010.
[32] A. Efraty, Closed circuit desalination series no-6: conventional RO compared with the conceptually different new closed circuit desalination technology, Desal. Wat. Treat., 41 (2012) 279–295.
[33] Dow Liquid Separation, FILMTEC™ Reverse Osmosis Membranes, Technical Manual, System Design, 2011, pp. 72–102. Available at: http://msdssearch.dow.com
[34] N.Y. Yip, A. Tiraferri, W.A. Phillip, J.D. Schiffman, L.A. Hoover, Y.C. Kim, M. Elimelech, Thin-film composite pressure retarded osmosis membranes for sustainable power generation from salinity gradients, *Environ. Sci. Technol.*, 45 (2011) 4360–4369.
[35] A.P. Straub, N.Y. Yip, M. Elimelech, Raised the bar: Increased hydraulic pressure enables unprecedented high power density in pressure retarded osmosis, Environ. Sci. Technol. Lett., 1 (2014) 55–59.
[36] S. Chou, R. Wang, L. Shi, Q. She, C. Tang, A.G. Fane, Thin-film hollow fiber membrane for pressure retarded osmosis (PRP) process with high power density, J. Membr. Sci., 389 (2012) 25–33.
[37] S. Zhang, T.S. Chung, Minimizing the instant and accumulation effects of salt permeability to sustain ultrahigh osmotic power density, Environ. Sci. Technol., 47 (2013) 10085–10092.
[38] C.F. Wan, T.S. Chung, Osmotic power generation by pressure retarded osmosis using seawater brine as the draw solution and wastewater retentate as the feed, J. Membr. Sci., 479 (2015) 148–158.
[39] X. Song, Z. Liu, D.D. Sun, Energy recovery form concentrated seawater brine by thin-film nanofiber composite pressure retarded osmosis membranes with high power density, Energy Environ. Sci., 6 (2013) 1199–1210.
[40] Y.C. Kim, M. Elimelech, Potential of osmotic power generation by pressure retarded osmosis using seawater as feed solution: analysis and experiments, J. Membr. Sci., 429 (2013) 330–337.
[41] Hydration Technology Innovations, HTI, Albany, NY, USA. Available at: http://www.htisater/
[42] Information on the GWRS Program in West Orange District, California, USA. Available at: http://www.gwrsystem.com
[43] Information on "NEWater" Production in Singapore. Available at: http://pub.gov.sg/water/newater
[44] K.H. Mistry, R.K. McGovern, G.P. Thiel, E.K. Summers, S.M. Zubair, J.H. Lienhard, Entropy generation analysis of desalination technologies, Entropy, 13 (2011) 1829–1864.
[45] http://civil.Coloardo.edu/~silverst2110/RANKINE%20POWER%20AND%20VCRCYCLES.pdf
[46] S.H. Kim, D.I. Kim, Scaling-up and piloting of pressure-retarded osmosis, Desal. Water Reuse, (2014) 36–38.
[47] A. Efraty, R.N. Barak, Z. Gal, Closed circuit desalination – a new low energy high recovery technology without energy recovery, Desal. Wat. Treat., 31 (2011) 95–101.
[48] A. Efraty, R.N. Barak, Z. Gal, Closed circuit desalination series no-2: new affordable technology for sea water desalination of low energy and high flux using short modules without need of energy recovery, Desal. Wat. Treat., 42 (2012) 189–196.
[49] A. Efraty, Closed circuit desalination series no-8: record saving of RO energy by SWRO-CCD without need of energy recovery, Desal. Wat. Treat., 52 (2014) 5717–5730.
[50] A. Efraty, CCD series No-11: single module compact SWRO-CCD units of low energy and high recovery for seawater desalination including with solar panels and wind turbines, Desal. Wat. Treat., 53 (2015) 1162–1176.
[51] A. Efraty, CCD series No-13: illustrating low energy SWRO-CCD of 60% recovery and BWRO-CCD of 92% recovery with a single element module without ER means – a theoretical extreme case study, Desal. Wat. Treat., 57 (2016) 9148–9165.
[52] A. Efraty, CCD series No-14: illustration of SWRO-CCD with fixed-pressure and variable flow instead of fixed-flow and variable pressure conditions, Desal. Wat. Treat., 56 (2015) 875–893.
[53] A. Efraty, CCD series No-15: simple design batch SWRO-CCD units for high recovery and low energy without ERD over a wide flux range of high cost effectiveness, Desal. Wat. Treat., 57 (2016) 9166–9179.
[54] A. Efraty, CCD series No-16: opened versus closed circuit SWRO batch desalination for volume reduction of silica containing effluents under super-saturation conditions, Desal. Wat. Treat., 57 (2016) 9569–9584.
[55] Z. Gal, A. Efraty, CCD series No-18: record low energy in closed circuit desalination of ocean seawater with nanoH_2O elements without ERD, Desal. Wat. Treat., 57 (2016) 9180–9189.
[56] J. Septon, A. Efraty, CCD series No-17: application of the BWRO-CCD technology for high recovery low energy desalination of domestic effluents, Desal. Wat. Treat., 57 (2016) 9585–9601.
[57] B. Mansell, T. Nikonova, P. Ackman, B. Langpap, C.C. Tang, R. Tremblay, P. Friess, Evaluation of RO Concentrate Treatment and Disposal Options for the Santa Clarita Valley, 29th Annual WateReuse Symposium, Dallas, TX, USA, 2014.